Received: 15 May 2023 | Revised: 19 July 2023 | Accepted: 20 July 2023

DOI: 10.1111/jace.19382

Journal of the American Ceramic Society

FINALIST ARTICLE

Polarity effects on wake-up behavior of $Al_{0.94}B_{0.06}N$ ferroelectrics

Keisuke Yazawa[1,2] | **Daniel Drury**[2,3] | **John Hayden**[4] | **Jon-Paul Maria**[4] | **Susan Trolier-McKinstry**[4] | **Andriy Zakutayev**[1] | **Geoff L. Brennecka**[2]

[1] Materials Science Center, National Renewable Energy Laboratory, Golden, Colorado, USA

[2] Department of Metallurgical and Materials Engineering, Colorado School of Mines, Golden, Colorado, USA

[3] U.S. Army Combat Capabilities Development Command—Army Research Laboratory, Adelphi, Maryland, USA

[4] Department of Materials Science and Engineering and the Materials Research Institute, The Pennsylvania State University, University Park, Pennsylvania, USA

Correspondence
Keisuke Yazawa and Geoff L. Brennecka, Materials Science Center, National Renewable Energy Laboratory, Golden, CO 80401, USA.
Email: Keisuke.Yazawa@nrel.gov and geoff.brennecka@mines.edu

Funding information
Division of Materials Research, Grant/Award Number: DMR-2119281; Basic Energy Sciences, Grant/Award Number: Early Career Award; Defense Sciences Office, DARPA, Grant/Award Numbers: DARPA-PA-19-04-03, HR0011-20-9-0047, W911NF-20-20274; Energy Frontier Research Centers, Grant/Award Number: DE-SC0021118

Editor's Choice
The Editor-in-Chief recommends this outstanding article.

Abstract

Wurtzite ferroelectric materials are promising candidates for energy-efficient memory technologies, particularly for applications requiring high operating temperatures. Asymmetric wake-up behaviors, in which the polarization reversal depends both on polarity and cycle number for the first few dozen cycles, must be better understood for reliable device operation. Here, the detailed analysis of the asymmetric wake-up behavior of thin film $Al_{0.94}B_{0.06}N$ was performed combining time-resolved switching measurements with Rayleigh analysis, piezoelectric measurements, and etching experiments of progressively switched samples. The analysis shows that the gradual opening of the polarization hysteresis loops associated with wake-up is driven by a gradual increase in the domain-wall density and/or domain-wall mobility with electric field cycle to the polarity opposite to the growth polarity. The insights of this discovery will help to guide interface and polarity design in the eventual deployment of reliable devices based on these materials.

KEYWORDS

ferroelectricity/ferroelectric materials, magnetron, nitrides, piezoelectric materials/properties, polarization, sputtering

1 | INTRODUCTION

Ferroelectric materials are ubiquitous across electronic technologies in the form of capacitors, piezoelectric actuators/sensors, energy harvesters, nonlinear optics, pyroelectric sensors, and positive temperature coefficient of resistance thermistors.[1–6] Thin film ferroelectrics have further enabled integrated devices such as ferroelectric random access memory and piezoelectric microelectromechanical systems.[7,8] Ferroelectric research is also vibrant for multiferroic[9] and photovoltaic[10,11] properties and the possibility of negative capacitance,[12] and new concepts keep emerging.[12–17] The development of new polar materials is of significant interest, and ferroelectricity has recently been observed or predicted in several crystal compositions, including fluorite (Hf,Zr)O_2,[18] wurtzite (Al,Sc)N,[19] and nitride perovskite $LaWN_3$.[19–23]

Among the newly discovered ferroelectric material classes, the wurtzite-structured ferroelectrics have enhanced piezoelectric response relative to AlN,[24] robust ferroelectricity with large spontaneous polarization,[19,25] and compatibility with both Si and III-N semiconductor technologies. Starting from (Al,Sc)N,[19] other chemistries such as (Al,B)N, (Zn,Mg)O, and (Ga,Sc)N have been reported to be ferroelectric.[25–27] The mechanism and origin of the wurtzite ferroelectrics are being intensely investigated with the goal to control the ferroelectric properties and discover novel ferroelectric materials.[19,28–35] . However, many questions remain, including the existence or absence of a Curie temperature, the domain boundary structure,[36] and the switching pathway.[37]

Polarization reorientation is the defining feature for ferroelectrics and is used in many of the abovementioned devices. Reliable operation of devices that depend upon polarization reversal requires understanding polarization switching characteristics associated with kinetics, fatigue, retention, and—for some systems—wake-up, which is the remanent polarization increase depending on cycle number for the first few dozen cycles. The newly discovered HfO_2- and AlN-based ferroelectrics often exhibit wake-up, which is considered a critical issue for device operation.[38–41] Although wake-up behavior is influenced by material chemistry, deposition process, electrode material, and measurement condition, domain-wall pinning and domain evolution during the voltage cycle are believed to be universally important.[42–45]

There has been a recent publication discussing the role of domain evolution in thin film (Al,B)N on the observed wake-up behavior.[41] However, detailed analysis on the domain evolution for each polarity with respect to growth polarity is still incomplete. One key feature of the wurtzite-structured materials is alignment of the polar axis during growth (i.e., nitrogen-polar or metal-polar), as opposed to the mixed-polarity or even random crystallographic orientation commonly seen in other ferroelectrics. This strong preference for growth polarity during deposition suggests that the relationship between growth polarity and switching polarity may influence the wake-up behavior of such materials.

In this study, it is demonstrated that polarization switching to the polarity opposite of the growth polarity is critical to the observed wake-up behavior of thin film $Al_{0.94}B_{0.06}N$. The polarization switching curve is orders of magnitude slower for the transition from the growth polarity to the antiparallel polarization state than going from antiparallel state back to the growth polarity. The domain-wall density and/or domain-wall mobility for switching from the antiparallel state to the growth polarity gradually increases with the number of cycles, causing the measured remanent polarization to increase for electric fields just above the coercive field, resulting in the observed wake-up behavior. Reversible and irreversible Rayleigh coefficients, piezoelectric coefficients, and chemical etching results reveal the domain structure and its evolution with the number of electric field cycles. These are consistent with the domain states predicted by the nucleation time and domain-wall velocity from switching kinetics studies on the same films.[35,41]

2 | EXPERIMENTAL PROCEDURES

2.1 | Sample synthesis

A 247 nm $Al_{0.94}B_{0.06}N$ film was deposited on W/c-sapphire via magnetron co-sputtering using the following growth conditions: 2 mTorr of Ar/N_2 (5/15 sccm flow), with target power densities of 12.5 W/cm2 (pulsed DC) on a 2″ diameter Al target (Kurt J. Lesker) and 4.75 W/cm^2 (RF) on a 2″ diameter BN target (Kurt J. Lesker). The substrate was rotated and heated to 325°C during deposition. The chamber base pressure at deposition temperature was $< 5 \times 10^{-7}$ Torr.

Top Au (100 nm)/Ti (5 nm) contacts 50 and 200 μm in diameter were deposited on the $Al_{0.94}B_{0.06}N$ film via electron beam evaporation through a photolithographic pattern.

2.2 | Measurements

Ferroelectric polarization—electric field hysteresis loop measurements were taken with a Precision Multiferroic system from Radiant Technologies. The applied triangle excitation field was 6.7 MV/cm at 10 kHz.

The polarization switching curves were measured with the switching current extracted by positive-up—negative-down (PUND) measurements,[46,47] namely, by subtracting the current signal associated with the second same-polarity pulse (including capacitive current and resistive current) from that of the first pulse (including switching current, capacitive current, and resistive current). The voltage pulses were applied through a top electrode, and the current flowing was measured using a transimpedance amplifier connected to the bottom electrode (Figure 1a). The details of the custom measurement system designed to cover $< \pm 200$ V and > 200 ns measurement range to observe sample-limited ferroelectric switching in

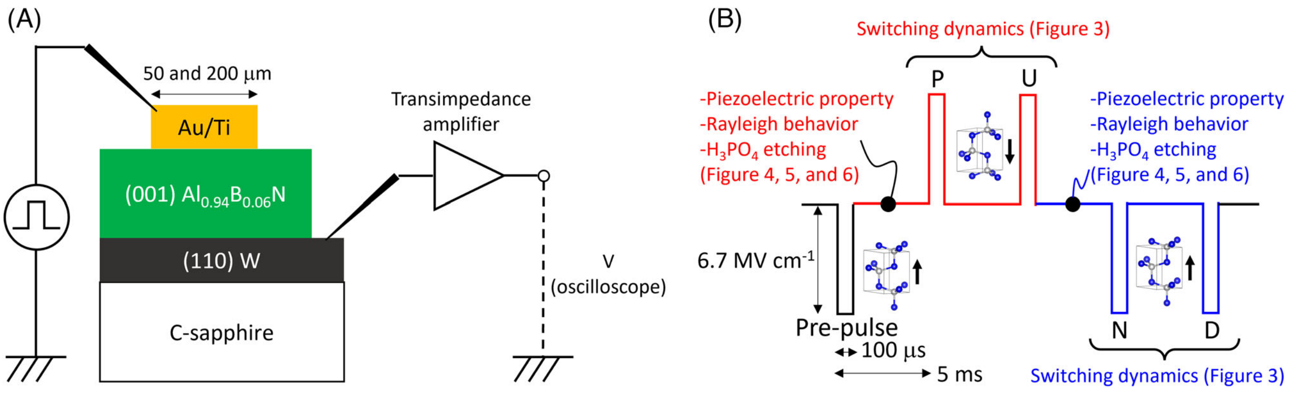

FIGURE 1 Schematic of PUND measurement setup: (a) diagram for connection between sample, pulse generator, and sensing amplifier; (b) pulse sequence programmed in pulse generator for each cycle of the PUND measurement.

sub-microsecond order was reported elsewhere.[48] In the current study, pulse sequences of 200 Hz with a duty cycle (i.e., the field-on:field-off ratio) of 2% and amplitude of 6.7 MV/cm were applied to the sample.

Cycling dependence of switching kinetics, Rayleigh behavior, piezoelectric properties, and chemical etching were acquired following sequential PUND pulses as shown in Figure 1b. Polarization switching curves were measured from the difference of the current flowing under P (or N) and U (or D) pulses at each cycle. Following the standard PUND procedure, an initial "preset" pulse was applied before the P pulse for each cycle to set the sample in a known state prior to the PUND cycle; thus, the film state prior to a P pulse should not be confused with the virgin, as-grown state. Rayleigh behaviors observed with various amplitudes of AC voltage (10 kHz) were linearly-fitted to determine the irreversible Rayleigh coefficients at the state prior to P and N pulses for each cycle. Effective piezoelectric $d_{33,\text{eff}}$ coefficients were measured using a double-beam laser interferometer from aixACCT at the state prior to P or N pulses for each cycle. Phosphoric acid etching (85°C for 10 min) and surface SEM observation (JEOL 7000F, acceleration voltage 10 kV) were carried out for six distinct capacitor devices on the single film. Those devices underwent PUND cycles stopping at the state prior to P and N pulses for 2, 5, and 20 cycles. Before the phosphoric acid etching, the top electrodes were removed by 1% HF etching for 2 h. There was no significant change in the film after the HF etching, in good agreement with the slow HF etching rate of AlN.[49]

3 | RESULTS

3.1 | Polarization–field (*P–E*) loops

Thin film $Al_{0.94}B_{0.06}N$ exhibits significant wake-up behavior in polarization—electric field (*P–E*) loops as shown in Figure 2. The *P–E* loops shown in Figure 2a (and Figure S1) were taken with repeated electric field excitation (10 kHz triangular wave with 6.7 MV/cm, 110% of the coercive field of the film defined by $(+E_c+(-E_c))/2$ after the wake-up under the primary measurement conditions used here. The *P–E* hysteresis loops gradually open with increasing number of cycles.

The remanent polarization values extracted from the *P–E* loops indicate that more than 20 cycles are required to saturate the hysteresis loops under these measurement conditions (Figure 2b). The positive side of the loops exhibit clear and sharp saturation throughout the wake-up process, implying that the downward polarity with respect to the laboratory reference frame shown in Figure 1a corresponding to a nitrogen polar film surface initially dominates the film and is gradually replaced with an upward poled (metal polar) state under applied negative electric field with an increasing number of cycles.

Figure 2c presents the positive and negative coercive fields after hysteresis saturation (> 20 cycles) extracted from the *P–E* loops. The negative coercive field is larger than the positive coercive field. In addition, the negative coercive field decreases with the number of cycles whereas the positive coercive field slightly increases. These results suggest the transition to metal polar from nitrogen polar under a negative electric field controls the wake-up behavior. The wake-up behavior is drive-amplitude dependent; that is, the larger the amplitude, the fewer cycles required for wake-up as shown in Figure S2.

3.2 | Time-dependent polarization

To understand the wake-up behavior in both polarities, the time-dependent polarization evolution under P and N pulses (Figure 3) was directly examined. This is because the *P–E* loops plotted in Figure 2a do not explicitly include any information about the time dependence of the

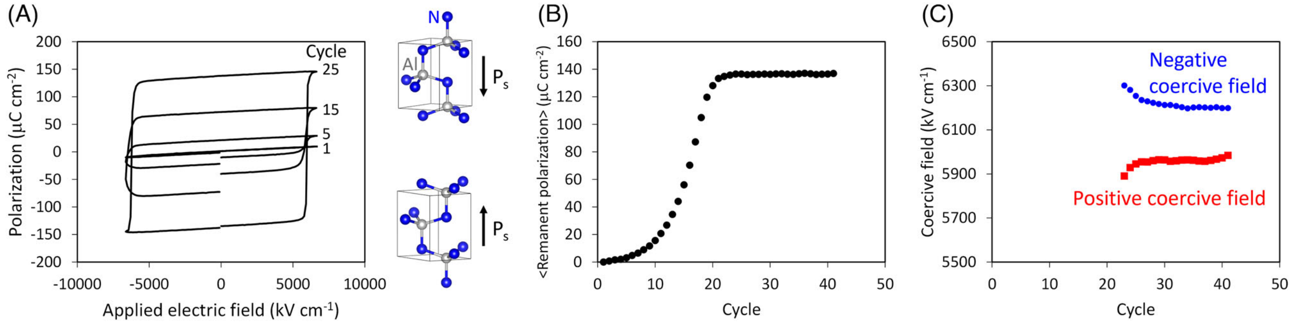

FIGURE 2 Wake-up behavior of thin film $Al_{0.94}B_{0.06}N$; all loops are centered on the polarization axis: (a) cycle dependence of polarization—electric field curves measured using 6.7 MV/cm 10 kHz triangular excitation; (b) average remanent polarization ((+Pr+(−Pr)/2) as a function of number of cycles showing that polarization wake-up takes >20 cycles to reach steady state switching for the excitation condition; and (c) observed coercive fields during the wake-up process.

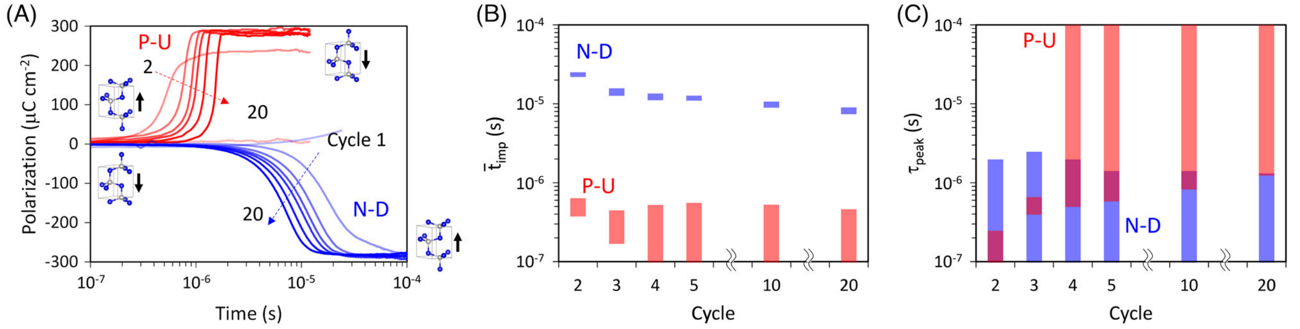

FIGURE 3 Polarization switching kinetics for both polarities: (a) cycle dependence of polarization evolution; (b) extracted $\bar{t}_{\text{imp}}$ as a function of number of cycles. $\bar{t}_{\text{imp}}$ from N–D pulses is orders of magnitudes larger than that from P–U pulses. (c) Extracted τ_{peak} as a function of number of cycles, whereas τ_{peak} from N–D pulses is invariant with cycle number, that from P–U increases with cycles.

polarization reversal process. Figure 3a illustrates the cycle dependence of the switching polarization during each pulse (red: polarization extracted from current during P–U pulses, blue: polarization from N–D pulses). There is no significant switching during the first cycle for either polarity. For cycles 2 and beyond, the polarization curves from the N–D pulses transitioning the polarity of the film to upward polarity (metal polar) from downward polarity (nitrogen polar) gradually shift toward faster times. Meanwhile, the polarization curves from the P—U pulses transitioning the polarity of the film to downward polarity (nitrogen polar) from upward polarity (metal polar) shift toward slower times. The absolute transition times of the polarization curves from the N—D pulses are consistently slower than that from the P—U pulses, suggesting the polarization switching under N—D is less favorable. This is consistent with the initial polarity (nitrogen polar) and decrease in coercive field at the negative electric field with cycles observed in Figure 2a,c.

The polarization switching curve can be fitted with a simultaneous nucleation and growth model[35] to analyze the competition of nucleation and growth. From the fitting, one can identify the nucleation rate peak time τ_{peak} expressed as[35]

$$\tau_{\text{peak}} = m\sqrt{\frac{m-1}{m\alpha}} \tag{1}$$

where m stands for mth-order nucleation rate, and α is a constant determining the peak position time. Also, the average impingement time $\bar{t}_{\text{imp}}$ is calculated with the following equation[35]:

$$\bar{t}_{\text{imp}} = \frac{1}{2v\sqrt{dN(\infty)}} \tag{2}$$

where v is the domain-wall velocity, d is the thickness, and $N(\infty)$ is the saturated density of nuclei. As seen in Equation (2), the average impingement time is closely related to both the growth velocity and saturated density of nuclei.

Figure 3b,c shows the fittable ranges of the $\bar{t}_{\text{imp}}$ and τ_{peak} for the experimental polarization curves, which can provide mechanistic insight about the cycle dependence of the polarization-switching curves and the wake-up

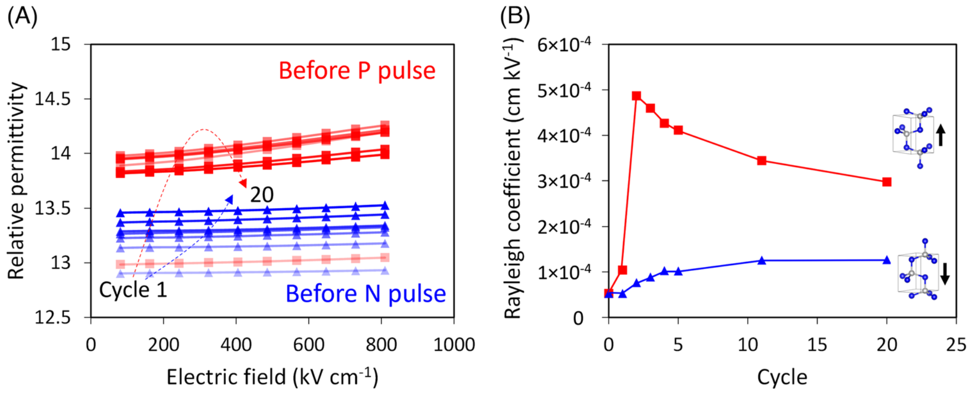

FIGURE 4 Rayleigh behavior for each cycle at states prior to P and N pulses: (a) relative permittivity increases with AC electric field amplitude, suggesting irreversible domain wall motion. Slopes of the curves vary with the number of cycles. (b) Irreversible Rayleigh coefficients, α, extracted from the slopes of the curves. Cycling dependence curves have opposite trends depending on the polarity.

behavior. Note that each experimental curve can be fit with a range of $\bar{\tau}_{imp}$ and τ_{peak} values.[35] Both polarities exhibit a reduction in $\bar{\tau}_{imp}$ with a number of cycles that indicates the domain-wall velocity and/or the saturated number of nuclei $vN(\infty)^{1/2}$ increases with cycle, implying either or both the domain-wall velocity and saturated density of nuclei increase. The nucleation rate peak τ_{peak}, however, shows different trends depending on the polarity of the reversal. The τ_{peak} associated with N—D (metal → nitrogen polarity) pulses is invariant of the number of cycles, whereas that from P—U (nitrogen → metal polarity) pulses increases with cycling. The root cause of the P—U curve shift to slower times with cycles seen in Figure 3a is the reduction in the nucleation rate. Those results suggest that the gradual $\bar{\tau}_{imp}$ reduction (increased domain-wall velocity) resulted in slower transition curves from the N—D pulses is associated with the wake-up behavior seen in the *P–E* loops. The switching curve shift to faster time under the N—D pulses corresponds to a reduction in coercive field in the negative lobe of the *P—E* loops with the number of cycles, as it is common for polarization reversal to have a strong dependence on field above E_c.[35,50,51]

3.3 | Cycle dependence of permittivity and Rayleigh coefficient

The decrease in nucleation rate for the polarization switching curves under P—U pulses and increase in domain-wall velocity or the saturated density of nuclei for polarization switching curves under the N—D pulses are consistent with the Rayleigh response[52,53] measured in this study. Figure 4a illustrates the cycle dependence of the relative permittivity as a function of AC electric field amplitude prior to each P (red) and N (blue) pulse. The curves show the increase in relative permittivity with both cycles and AC electric field amplitude attributed to domain-wall contributions driven by an electric field. The slopes of the curves, irreversible Rayleigh coefficients that represent the field-driven domain-wall motion going over the domain pinning energy barriers, are extracted and plotted in Figure 4b.

The irreversible Rayleigh coefficients in both polarities increase as the film is cycled, which is in good agreement with a previous wake-up study,[41] although the specific behavior for each polarity is different. A monotonic increase in the irreversible Rayleigh coefficients is seen in the state before N pulses (nitrogen polar), whereas a peak of the irreversible Rayleigh coefficients is observed in the state before P pulses (metal polar). The monotonic increase in the state before N pulses can originate from either the monotonic increase in the domain-wall velocity or existing domain-wall density associated with existing nuclei at the stage prior to N pulses. The reversible Rayleigh coefficients, which is the relative permittivity intercepts at $E = 0$, also substantially increase with the number of cycles (Figure 4a). The reversible Rayleigh coefficients represent the sum of the intrinsic response and the reversible domain-wall motion within each potential well of spatially distributed pinning centers.[52] Long-range movement of reversible domain walls is not significant because the walls remain pinned, so that the increase of the reversible Rayleigh coefficient implies the domain-wall density increases with cycles. This discussion provides an insight that the monotonic increase in the coupled parameter $vN(\infty)^{1/2}$ (or decrease in $\bar{\tau}_{imp}$) seen in Figure 3b originates at least in part from an increase in the saturated nucleus density $N(\infty)$ caused by the increase in the number of existing nucleation sites; it is also possible that the velocity changes.

The peak in irreversible Rayleigh coefficients observed in the state before P pulses can be attributed to both the

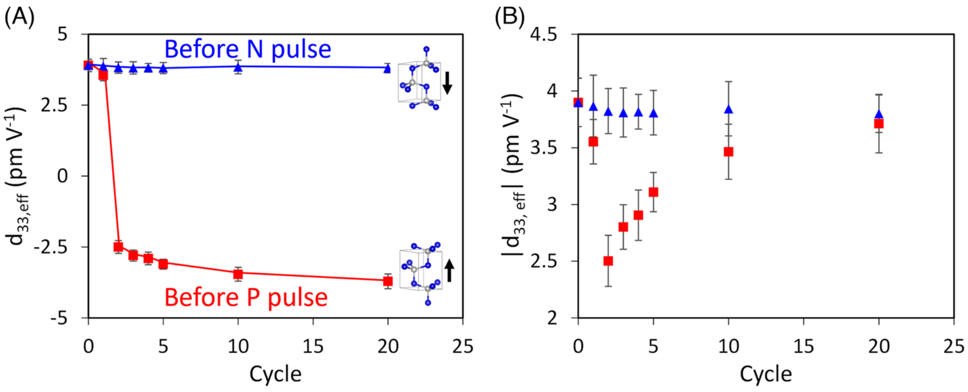

FIGURE 5 Cycling dependence of piezoelectric properties for states prior to P and N pulses: (a) evolution of effective piezoelectric coefficients for each polarity with cycle number; (b) the gradual increase of the absolute value of effective piezoelectric coefficient with cycles for the state prior to P pulses and convergence with the value for the state prior to N pulses that shows no significant change with a number of cycles.

large domain-wall density and domain-wall velocity, but the domain-wall density is likely the main origin given the decrease of the irreversible Rayleigh coefficients at >2 cycles and increase in the reversible Rayleigh coefficients. The decrease in the irreversible Rayleigh coefficient with cycles > 2 reflects the nucleation rate peak time shown in Figure 3c. This gives an insight that the domain walls and antiparallel domains exist in significant numbers compared to the other polarity (before N pulses) even before applying P pulses (cycle >2) and accelerate the nucleation rate.[35]

3.4 | Cycle dependence of piezoelectric coefficient

The presence of preexisting domain walls from pre-pulse before the P pulse are confirmed via piezoelectric property measurements. The wurtzite crystallography allows only two possible polarization directions $[0\,0\,0\,1]$ and $[0\,0\,0\,\bar{1}]$, and the high degree of texture of these films[19,54,55] as seen in the XRD profile of the film (Figure S3) justifies the focus on only two domain states. Existence of antiparallel domains would both introduce 180° domain walls and reduce the measured piezoelectric response. Figure 5a shows the cycle dependence of the measured piezoelectric coefficients prior to each P (red) and N (blue) pulse. Before N pulses, the coefficient is positive due to the downward polar (nitrogen polar) state that is in phase with the applied electric field. Before P pulses, the coefficient is negative due to the upward polar (metal polar) state (at cycle >2) that is opposite to the applied electric field phase. Before the first P pulse, the coefficient is positive because the film does not undergo the polarization switching to metal polar from nitrogen polar, which is in good agreement with the polarization evolution and Rayleigh behavior shown in Figures 3a and 4a. Those behaviors are consistent with the cycle dependence of the polarization evolution and Rayleigh behavior.

The measured piezoelectric coefficients illuminate the mixed polar state followed by the pre-pulse prior to the P pulses. Figure 5b shows effective piezoelectric coefficients for cycle >2 prior to each P (red) and N (blue) pulse. The effective piezoelectric coefficients prior to N pulses show no significant change with the number of cycles. This result indicates the volume of the antiparallel domains associated with an increase in the domain-wall density (confirmed in the Rayleigh coefficient, Figure 4a,b) is not significant enough to affect the effective piezoelectric coefficients within the error of the measurements.

As for the state prior to P pulses, there is a significant increase in the measured piezoelectric coefficient observed. The effective piezoelectric coefficient eventually reaches values similar to that of the state prior to N pulses at 20 cycles. These behaviors indicate that the polar mixture state exists prior to the P pulses and dissolves with cycling. The state prior to the N pulses does not have a significant polar mixture state. These results are consistent with the cycle dependence of the nucleation rate peak position, and Rayleigh behavior and support the assertion that a fast nucleation rate assisted by existing domain walls at the state followed by the pre-pulse plays the key role in the fast switching under P—U pulses at lower cycle numbers.

3.5 | Location of antiparallel domains

The next question is where the domain walls and associated 180° domains arising at the timing followed by the pre-pulse and before the P pulse are located. AlN-based films exhibit polarity selectivity to hot phosphoric acid, so chemical etching (see Section 2) combined with plan-view

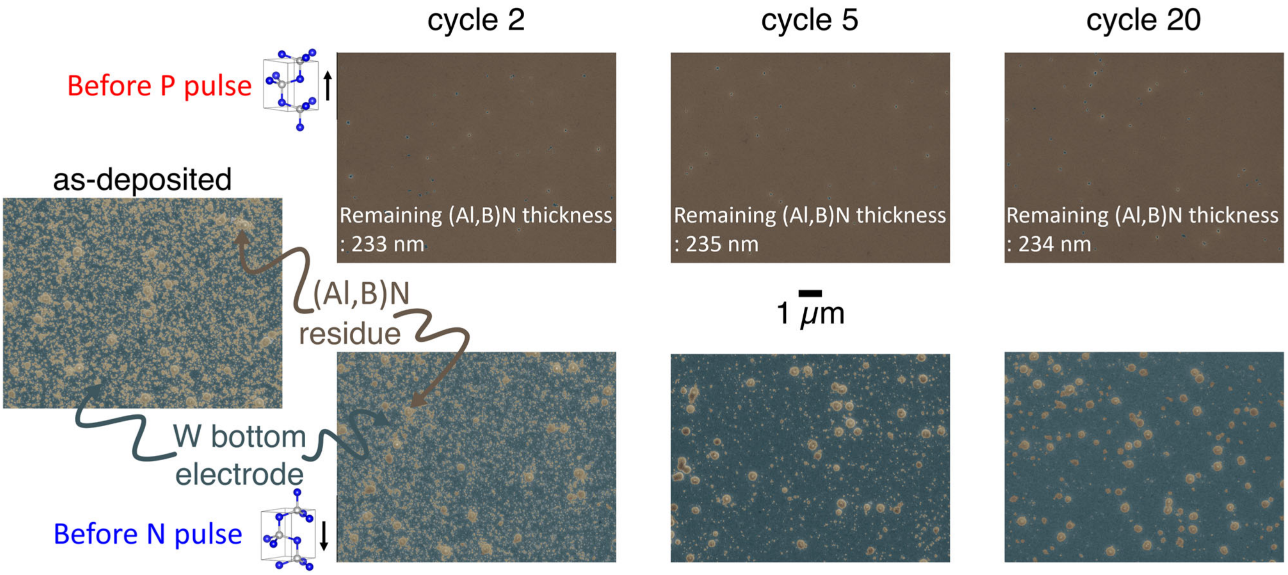

FIGURE 6 SEM images of $Al_{0.94}B_{0.06}N$ films after phosphoric acid etching following various numbers of PUND switching cycles. States prior to P pulses are highly M-polar, and little etching takes place regardless of cycle number. Prior to N pulses, films are majority N-polar, leading to rapid etching and exposure of the bottom W electrode. A gradual reduction in the volume of a post-etching film residue with cycle number suggests a corresponding reduction in mixed-polarity state. The color and contrast of the images are emphasized to visually distinguish between the film residue and exposed W electrode.

SEM observation provides a complementary method to observe film polarity prior to the P and N pulses (Figure 6).

As-deposited films and those before N pulses etched completely in 10 min, consistent with the fast etch rate of the nitrogen polar state, and the underlying W electrode is exposed. The as-deposited polar state is consistent with the *P*–*E* loops (Figure 1a) and piezoelectric measurements (Figure 5a). The film residue decreases with increasing cycles under N pulses, supporting the related discussion that the antiparallel domain volume associated with the domain-wall density at the states followed by U pulses prior to N pulses is small as seen in the piezoelectric measurements (Figure 5b). Prior to a P pulse, the film should be in a (majority) metal-polar state, which etches slowly. Consistent with this, such films remain ~235 nm thick (i.e., ~15 nm etched, measured with a profilometer) regardless of a number of cycles >2, which indicates that there is no significant difference in the polarity at the top electrode/film interface as a function of the number of cycles.

Given those etching results and facts that the polarization evolution, Rayleigh behavior, and piezoelectric measurements consistently indicate the presence of domain walls after the preset pulses and before the P pulses, it is concluded that nitrogen polar domains are located in the vicinity of the film/bottom electrode interface and do not pass completely through the thickness. Indeed, Wolff et al. reported a few nm layer of an antiparallel polar region at the interface between the bottom electrode and (Al,Sc)N thin film after a polarization switching event.[54] In the wake-up process (<5 cycles) shown in this study, the volume of the nitrogen polar domains in the macroscopically metal polar state prior to P pulses is larger than a few nm layer given the 20%–35% decrease of effective piezoelectric coefficient. Under P pulses during the wake-up cycle, emerging nitrogen polar domains likely nucleate from the preexisting domains, which facilitates the polarization switching at <5 cycles as seen in Figure 3a.

4 | DISCUSSION

The self-consistency of the previous results supports the comprehensive mechanistic model of the switching and wake-up behavior shown in Figure 7. Following the preset pulse but prior to P pulses, there exist nitrogen polar domains at the film/W interface, as evidenced by the large reversible and irreversible Rayleigh coefficients (Figure 4a,b), cycle-dependent piezoelectric measurements (Figure 5b), and etching results (Figure 6); these serve as nucleation sites for subsequent switching as shown schematically in Figure 7a. As the number of cycles is increased, the volume of these pre-pulse-induced nitrogen-polar domains and associated domain walls decrease as seen in the Rayleigh behavior (Figure 4b) and piezoelectric measurements (Figure 5b), and correspondingly, the nucleation rate peak position shifts later and later in time (Figure 3c). This leads to a slower overall polarization switching transition at higher cycle numbers (Figure 3a) even though the impingement time becomes

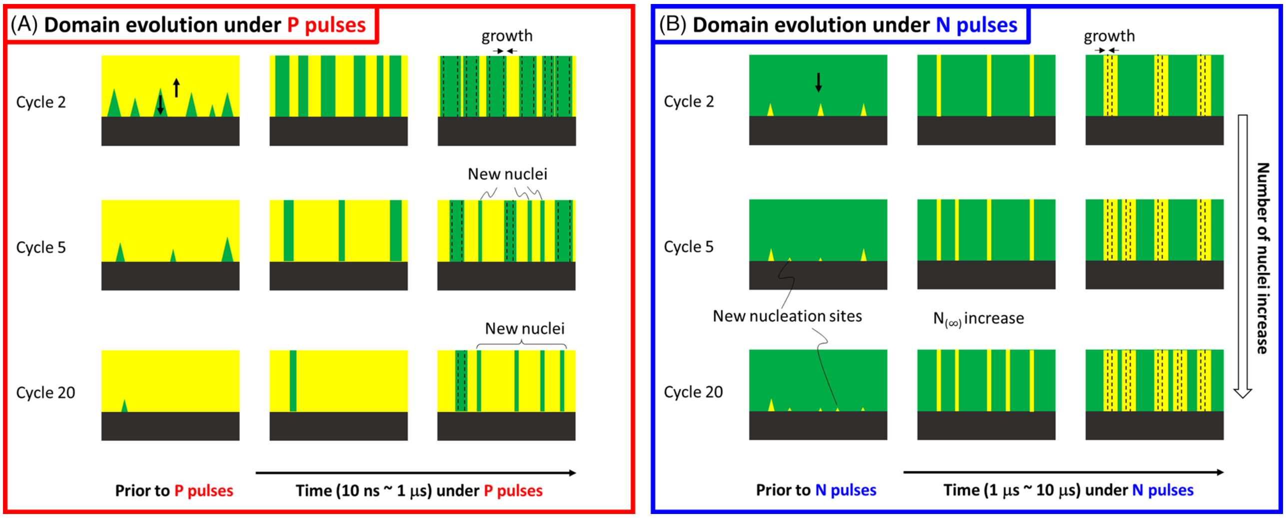

FIGURE 7 Schematic of domain (a) at state followed by pre-pulse prior to P pulses, and under P pulses, and (b) at state followed by U pulse prior to N pulses. Yellow regions represent upward polarity (metal polar) and green represents downward polarity (nitrogen polar). Fast transition under P pulses does not contribute to wake-up, whereas the gradual domain wall density and/or velocity during the slow transition under N pulses play a key role in wake-up behavior.

faster with increased cycles (Figure 3b) as supported by the decreased irreversible Rayleigh coefficient (Figure 4b). However, the impingement time under P pulses is orders of magnitude faster than that under N pulses, so the domain evolution under P pulses does not contribute to the observed wake-up behavior.

Instead, wake-up behavior is dominated by domain evolution under N pulses as shown in Figure 7b. The slower switching kinetics of N pulses (Figure 3a) corresponds to the larger coercive field at a negative electric field for a given measurement frequency. The volume of metal polar domains prior to N pulses is insignificant as confirmed by the piezoelectric measurements (Figure 5b), and the residue after etching decreases with cycle number (Figure 6), whereas the number of the small nucleation sites increases (Figure 4a,b). After the N pulse is applied, domain nucleation occurs in ~1 μs (Figure 3c), and by ~10 μs, domain growth and impingement are essentially complete, and the saturated density of nuclei increases with number of cycles as evidenced in Figures 3b, 4a,b. This gradual increase in the saturated density of nuclei plays a key role in the wake-up behavior that is the gradual coercive field decrease at a negative electric field applied from the top electrode with cycles.

5 | CONCLUSION

In summary, the wake-up behavior associated with domain evolution of an $Al_{0.94}B_{0.06}N$ film is elucidated with a combination of polarization switching kinetics, Rayleigh analysis, piezoelectric measurements, and etching experiments for both polarities. The mixed polarity domains were observed prior to the transition to nitrogen polar (downward polarity) under the positive electric field pulses, at a fewer number of cycles. This mixed polarity state accelerates the switching transition. On the other hand, there was no significant density of mixed polarity domains observed prior to the transition to metal polar (upward polarity) under the negative electric field pulses regardless of the number of cycles, which causes slower switching kinetics than the transition to nitrogen polar under the positive electric field pulses. In addition, the domain-wall density increases with cycles, causing switching curves for the transition to the metal polar state to shift to faster times with increasing cycles, although the kinetics are still slower than the complementary transition to the nitrogen polar state. This gradual domain-wall density increase for the transition from nitrogen polar (growth polarity) to metal polar is the key origin of the wake-up behavior, as it drives a gradual decrease in coercive field for fixed switching parameters under a negative electric field during the wake-up process.

ACKNOWLEDGMENTS

This work was coauthored by Colorado School of Mines and the National Renewable Energy Laboratory, operated by the Alliance for Sustainable Energy, LLC, for the U.S. Department of Energy (DOE) under Contract No. DE-AC36-08GO28308. Funding was provided by the DARPA Tunable Ferroelectric Nitrides (TUFEN) program (DARPA-PA-19-04-03) as a part of Development and Exploration of FerroElectric Nitride Semiconductors (DEFENSE) project (electrical measurements and characterization), by the Office of Science (SC), Office of Basic Energy Sciences (BES) as part of the Early Career Award "Kinetic Synthesis of Metastable Nitrides" (data analysis and manuscript preparation), and by the National

Science Foundation under grant number DMR-2119281 (data analysis and manuscript preparation). Development of the $Al_{1-x}B_xN$ film growth methods was supported by grants DARPA, grants HR0011-20-9-0047 and W911NF-20-20274, whereas the film deposition was supported as part of the center for 3D Ferroelectric Microelectronics (3DFeM), an Energy Frontier Research Center funded by the U.S. Department of Energy (DOE), Office of Science, Basic Energy Sciences under Award Number DE-SC0021118. The data affiliated with this study are available from the corresponding author upon reasonable request. The views expressed in the article do not necessarily represent the views of the DOE or the U.S. Government.

CONFLICT OF INTEREST STATEMENT

The authors declare no conflicts of interest.

ORCID

Keisuke Yazawa https://orcid.org/0000-0002-5304-1696
Jon-Paul Maria https://orcid.org/0000-0003-3604-4761

REFERENCES

1. Uchino K. Ferroelectric devices. New York: Marcel Dekker; 2000
2. Burn I, Smyth DM. Energy storage in ceramic dielectrics. J Mater Sci. 1972;7(3):339–43. https://doi.org/10.1007/BF00555636
3. Muralt P. Ferroelectric thin films for micro-sensors and actuators: a review. J Micromechanics Microengineering. 2000;10(2):136–46. https://doi.org/10.1088/0960-1317/10/2/307
4. Sodano HA, Inman DJ, Park G. A review of power harvesting from vibration using piezoelectric materials. Shock Vib Dig. 2004;36(3):197–205. https://doi.org/10.1177/0583102404043275
5. Drdomenico M, Wemple SH. Oxygen-octahedra ferroelectrics. I. Theory of electro-optical and nonlinear optical effects. J Appl Phys. 1969;40(2):720–34. https://doi.org/10.1063/1.1657458
6. Lee MH, Guo R, Bhalla AS. Pyroelectric sensors. J Electroceramics. 1998;2(4):229–42. https://doi.org/10.1023/A:1009922522642
7. Scott JF, Paz De Araujo CA. Ferroelectric memories. Science (80–). 1989;246(4936):1400–5. https://doi.org/10.1126/science.246.4936.1400
8. Trolier-McKinstry S, Muralt P. Thin film piezoelectrics for MEMS. J Electroceramics. 2004;12:7–17.
9. Ramesh R, Spaldin NA. Multiferroics: progress and prospects in thin films. Nat Mater. 2007;6(1):21–9. https://doi.org/10.1038/nmat1805
10. Yang SY, Seidel J, Byrnes SJ, Shafer P, Yang CH, Rossell MD, et al. Above-bandgap voltages from ferroelectric photovoltaic devices. Nat Nanotechnol. 2010;5(2):143–7. https://doi.org/10.1038/nnano.2009.451
11. Kojima A, Teshima K, Shirai Y, Miyasaka T. Organometal halide perovskites as visible-light sensitizers for photovoltaic cells. J Am Chem Soc. 2009;131(17):6050–1. https://doi.org/10.1021/ja809598r
12. Hoffmann M, Fengler FPG, Herzig M, Mittmann T, Max B, Schroeder U, et al. Unveiling the double-well energy landscape in a ferroelectric layer. Nature. 2019;565(7740):464–7. https://doi.org/10.1038/s41586-018-0854-z
13. Yadav AK, Nelson CT, Hsu SL, Hong Z, Clarkson JD, Schlepütz CM, et al. Observation of polar vortices in oxide superlattices. Nature. 2016;530(7589):198–201. https://doi.org/10.1038/nature16463
14. Dai C, Stoica VA, Das S, Hong Z, Martin LW, Ramesh R, et al. Tunable nanoscale evolution and topological phase transitions of a polar vortex supercrystal. Adv Mater. 2022;34(11):2106401. https://doi.org/10.1002/adma.202106401
15. Qi Lu, Ruan S, Zeng YJ. Review on recent developments in 2D ferroelectrics: theories and applications. Adv Mater. 2021;33(13):2005098. https://doi.org/10.1002/adma.202005098
16. Ishiwara H, Aoyama Y, Okada S, Shimamura C, Tokumitsu E. Ferroelectric neuron circuits with adaptive-learning function. Comput Electr Eng. 1997;23(6):431–8. https://doi.org/10.1016/S0045-7906(97)00029-3
17. Oh S, Hwang H, Yoo IK. Ferroelectric materials for neuromorphic computing. APL Mater. 2019;7(9):091109. https://doi.org/10.1063/1.5108562
18. Böscke TS, Müller J, Bräuhaus D, Schröder U, Böttger U. Ferroelectricity in hafnium oxide thin films. Appl Phys Lett. 2011;99(10). https://doi.org/10.1063/1.3634052/121850
19. Fichtner S, Wolff N, Lofink F, Kienle L, Wagner B. AlScN: a III–V semiconductor based ferroelectric. J Appl Phys. 2019;125(11):114103. https://doi.org/10.1063/1.5084945
20. Fang YW, Fisher CAJ, Kuwabara A, Shen XW, Ogawa T, Moriwake H, et al. Lattice dynamics and ferroelectric properties of the nitride perovskite LaWN3. Phys Rev B. 2017;95(1):014111. https://doi.org/10.1103/PhysRevB.95.014111
21. Gui C, Dong S. Pressure-induced ferroelectric phase of $LaMoN_3$. Phys Rev B. 2020;102(18):180103. https://doi.org/10.1103/PhysRevB.102.180103
22. Talley KR, Perkins CL, Diercks DR, Brennecka GL, Zakutayev A. Synthesis of $LaWN_3$ nitride perovskite with polar symmetry. Science (80–). 2021;374(6574):1488–91. https://doi.org/10.1126/science.abm3466
23. Sherbondy R, Smaha RW, Bartel CJ, Holtz ME, Talley K R, Levy-Wendt B, et al. High-throughput selection and experimental realization of two new Ce-based nitride perovskites: $CeMoN_3$ and $CeWN_3$. Chem Mater. 2022;34(15):6883–93. https://doi.org/10.1021/acs.chemmater.2c01282
24. Akiyama M, Kamohara T, Kano K, Teshigahara A, Takeuchi Y, Kawahara N. Enhancement of piezoelectric response in scandium aluminum nitride alloy thin films prepared by dual reactive cosputtering. Adv Mater. 2009;21(5):593–6. https://doi.org/10.1002/adma.200802611
25. Hayden J, Hossain MD, Xiong Y, Ferri K, Zhu W, Imperatore MV, et al. Ferroelectricity in boron-substituted aluminum nitride thin films. Phys Rev Mater. 2021;5(4):044412.
26. Ferri K, Bachu S, Zhu W, Imperatore M, Hayden J, Alem N, et al. Ferroelectrics everywhere: ferroelectricity in magnesium substituted zinc oxide thin films. J Appl Phys. 2021;130(4):044101. https://doi.org/10.1063/5.0053755
27. Wang D, Wang P, Wang B, Mi Z. Fully epitaxial ferroelectric ScGaN grown on GaN by molecular beam epitaxy. Appl Phys Lett. 2021;119(11):111902. https://doi.org/10.1063/5.0060021
28. Yasuoka S, Shimizu T, Tateyama A, Uehara M, Yamada H, Akiyama M, et al. Effects of deposition conditions on the ferroelectric properties of $(Al_{1-x}Sc_x)N$ thin films. J Appl Phys. 2020;128(11):114103. https://doi.org/10.1063/5.0015281

29. Hayden J, Hossain MD, Xiong Y, Ferri K, Zhu W, Imperatore MV, et al. Ferroelectricity in boron-substituted aluminum nitride thin films. Phys Rev Mater. 2021;5(4):044412. https://doi.org/10.1103/PhysRevMaterials.5.044412
30. Yazawa K, Drury D, Zakutayev A, Brennecka GL. Reduced coercive field in epitaxial thin film of ferroelectric wurtzite $Al_{0.7}Sc_{0.3}N$. Appl Phys Lett. 2021;118(16):162903. https://doi.org/10.1063/5.0043613
31. Rassay S, Hakim F, Li C, Forgey C, Choudhary N, Tabrizian R. A segmented-target sputtering process for growth of sub-50 nm ferroelectric scandium–aluminum–nitride films with composition and stress tuning. Phys Status Solidi—Rapid Res Lett. 2021;15(5):2100087. https://doi.org/10.1002/pssr.202100087
32. Yazawa K, Zakutayev A, Brennecka GL. A Landau–Devonshire analysis of strain effects on ferroelectric $Al_{1-x}Sc_xN$. Appl Phys Lett. 2022;121(4):042902. https://doi.org/10.1063/5.0098979
33. Yazawa K, Mangum JS, Gorai P, Brennecka GL, Zakutayev A. Local chemical origin of ferroelectric behavior in wurtzite nitrides. J Mater Chem C. 2022;10(46):17557. https://doi.org/10.1039/d2tc02682a
34. Drury D, Yazawa K, Zakutayev A, Hanrahan B, Brennecka G. High-temperature ferroelectric behavior of $Al_{0.7}Sc_{0.3}N$. Micromachines. 2022;13(6):887. https://doi.org/10.3390/MI13060887
35. Yazawa K, Hayden J, Maria JP, Zhu W, Trolier-McKinstry S, Zakutayev A, et al. Anomalously abrupt switching of wurtzite-structured ferroelectrics: simultaneous non-linear nucleation and growth model. Mater Horizons. 2023;10(8):2936–2944. https://doi.org/10.1039/D3MH00365E
36. Calderon S, Hayden J, Baksa SM, Tzou W, Trolier-McKinstry S, Dabo I, et al. Atomic-scale polarization switching in wurtzite ferroelectrics. Science (80–). 2023;380(6649):1034–8. https://doi.org/10.1126/SCIENCE.ADH7670/SUPPL_FILE/SCIENCE.ADH7670_MOVIE_S1.ZIP
37. Lee CW, Din NU, Yazawa K, Brennecka GL, Zakutayev A, Gorai P. Emerging materials and design principles for wurtzite-type ferroelectrics. ChemRxiv. 2023. https://doi.org/10.26434/CHEMRXIV-2023-HF60W
38. Zhou D, Xu J, Li Q, Guan Y, Cao F, Dong X, et al. Wake-up effects in Si-doped hafnium oxide ferroelectric thin films. Appl Phys Lett. 2013;103(19):192904. https://doi.org/10.1063/1.4829064/129761
39. Jiang P, Luo Q, Xu X, Gong T, Yuan P, Wang Y, et al. Wake-up effect in HfO_2-based ferroelectric films. Adv Electron Mater. 2021;7(1):2000728. https://doi.org/10.1002/AELM.202000728
40. Wang D, Zheng J, Tang Z, D'Agati M, Gharavi PSM, Liu X, et al. Ferroelectric C-axis textured aluminum scandium nitride thin films of 100 nm thickness. In: Joint Conference of the IEEE International Frequency Control Symposium and International Symposium on Applications of Ferroelectrics (IFCS-ISAF). Institute of Electrical and Electronics Engineers Inc.; 2020. p. 1–4. https://doi.org/10.1109/IFCS-ISAF41089.2020.9234910
41. Zhu W, He F, Hayden J, Fan Z, Yang JI, Maria JP, et al. Wake-up in $Al_{1-x}B_xN$ ferroelectric films. Adv Electron Mater. 2021;8:2100931. https://doi.org/10.1002/aelm.202100931
42. Buragohain P, Richter C, Schenk T, Lu H, Mikolajick T, Schroeder U, et al. Nanoscopic studies of domain structure dynamics in ferroelectric La:HfO_2 capacitors. Appl Phys Lett. 2018;112(22):222901. https://doi.org/10.1063/1.5030562
43. Kim HJ, Park MH, Kim YJ, Lee YH, Moon T, Kim K, et al. A study on the wake-up effect of ferroelectric $Hf_{0.5}Zr_{0.5}O_2$ films by pulse-switching measurement. Nanoscale. 2016;8(3):1383–9. https://doi.org/10.1039/c5nr05339k
44. Marincel DM, Zhang H, Kumar A, Jesse S, Kalinin SV, Rainforth WM, et al. Influence of a single grain boundary on domain wall motion in ferroelectrics. Adv Funct Mater. 2014;24(10):1409–17. https://doi.org/10.1002/adfm.201302457
45. Yazawa K, Uchida H, Blendell JE. Origin of grain size effects on voltage-driven ferroelastic domain evolution in polycrystalline tetragonal lead zirconate titanate thin film. Adv Funct Mater. 2020;30(9):1909100. https://doi.org/10.1002/adfm.201909100
46. Yang SY, Zavaliche F, Mohaddes-Ardabili L, Vaithyanathan V, Schlom DG, Lee YJ, et al. Metalorganic chemical vapor deposition of lead-free ferroelectric $BiFeO_3$ films for memory applications. Appl Phys Lett. 2005;87(10):102903. https://doi.org/10.1063/1.2041830
47. Mihara T, Araujo HW. Evaluation of imprint properties in sol-gel ferroelectric $Pb(ZrTi)O_3$ thin-film capacitors. Jpn J Appl Phys. 1993;32(9):4168–74. https://doi.org/10.1143/JJAP.32.4168/XML
48. Yazawa K, Zakutayev A, Brennecka GL. High-speed and high-power ferroelectric switching current measurement instrument for materials with large coercive voltage and remanent polarization. Sensors. 2022;22(24):9659. https://doi.org/10.3390/s22249659
49. Walker P, Tarn W. CRC handbook of metal etchants. Boca Raton, FL, USA: CRC Press; 1990.
50. Merz WJ. Domain formation and domain wall motions in ferroelectric $BaTiO_3$ single crystals. Phys Rev. 1954;95(3):690–8. https://doi.org/10.1103/PhysRev.95.690
51. Jo JY, Han HS, Yoon JG, Song TK, Kim SH, Noh TW. Domain switching kinetics in disordered ferroelectric thin films. Phys Rev Lett. 2007;99(26):267602. https://doi.org/10.1103/PhysRevLett.99.267602
52. Boser O. Statistical theory of hysteresis in ferroelectric materials. J Appl Phys. 1987;62(4):1344–8. https://doi.org/10.1063/1.339636
53. Hall DA, Stevenson PJ. High field dielectric behaviour of ferroelectric ceramics. Ferroelectrics. 1999;228:139–58.
54. Wolff N, Fichtner S, Haas B, Islam MR, Niekiel F, Kessel M, et al. Atomic scale confirmation of ferroelectric polarization inversion in wurtzite-type AlScN. J Appl Phys. 2021;129(3):034103. https://doi.org/10.1063/5.0033205
55. Stolyarchuk N, Markurt T, Courville A, March K, Zúñiga-Pérez J, Vennéguès P, et al. Intentional polarity conversion of AlN epitaxial layers by oxygen. Sci Rep. 2018;2018 81. 8(1):1–8. https://doi.org/10.1038/s41598-018-32489-w

SUPPORTING INFORMATION

Additional supporting information can be found online in the Supporting Information section at the end of this article.

How to cite this article: Yazawa K, Drury D, Hayden J, Maria J-P, Trolier-McKinstry S, Zakutayev A, et al. Polarity effects on wake-up behavior of $Al_{0.94}B_{0.06}N$ ferroelectrics. J Am Ceram Soc. 2024;107:1523–1532. https://doi.org/10.1111/jace.19382